Optical Detection of a Highly Localized Impurity State in Monolayer Tungsten Disulfide

Toshiaki Kato* **and Toshiro Kaneko**

Department of Electronic Engineering, Tohoku University, Aoba 6-6-05, Aramaki, Aoba-Ku, Sendai, Japan

ABSTRACT A photoluminescence (PL) peak has been observed from a monolayer of transition metal dichalcogenide (TMD), which is known to be an ideal 2D semiconductor. The PL peak appears near the low-energy side of neutral free excitons with very sharp peak width (~10 meV) at low temperature (83 K). Systematic temperature-dependent PL measurements reveal that the peak can be explained by bound excitons being trapped by the surface impurities, which results in a highly localized state for the excitons. Since the optically detectable, highly localized impurity state promises to have extensive practical applications for quantum optics, our finding represents an important step in the study of 2D materials for use in quantum computation and information.

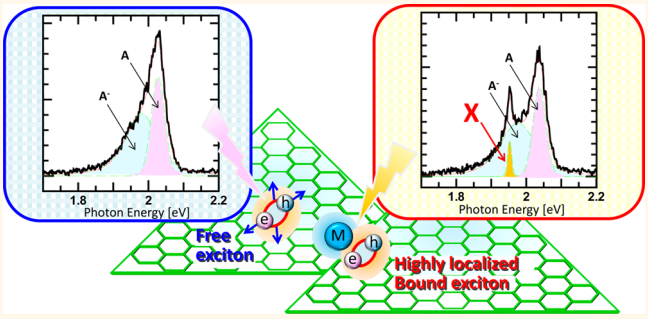

KEYWORDS: transition metal dichalcogenide · photoluminescence · bound exciton · impurity state

In the last two decades, atomically localized impurities in semiconductor materials have become a hot topic for the quantum scientific field because single impurities could be used as the "qubits" of quantum computation, as well as nonclassical light sources, in quantum information science.[1−3] Since the excitons trapped by the localized impurities have a long coherence length, photoluminescence (PL) spectra from such excitons are known to show very sharp peak width. The localized single impurities have been studied in many semiconductor materials, such as nitrogen-vacancy (NV) centers in diamond, isoelectronic tellurium impurity centers in ZnSe, and N pairs in GaP.[4−8] However, controlling the impurity state in order to obtain desirable and reproducible features still remains difficult since serious challenges, as well as significant contributions, are expected to arise from the investigation of ideal semiconductor materials with single impurities.[9] Transition metal dichalcogenide (TMD) is a semiconductor material with true two-dimensional (2D) atomic scale thickness.[10,11] In addition to this structural advantage, TMD includes many outstanding optical characteristics such as a clear band gap with direct optical transition, spin-valley coupling, and stable exciton and trion (charged exciton) states.[12−14] Despite those potentials of TMD in optical science and applications, the number of optical studies dealing with the impurity state in TMD is very small. The only PL feature related to defects in TMD was reported as a broad PL peak.[15] The optically detectable, highly localized impurity state in TMD has not been reported yet.

Here, we demonstrate the first optical detection for the localized-impurity state in TMD. The novel impurity states in PL spectra show very narrow peak width ($\Gamma_{PL} \approx 10$ meV) and small energy shift ($\Delta E_{PL} \approx 100$ meV) from the neutral excitons at low temperature (83 K), which is completely different from the previously reported features ($\Gamma_{PL} \approx 200$ meV, $\Delta E_{PL} \approx 200$ meV) of defect-induced PL in TMD.[15] Systematic PL investigations revealed that the observed peak can be explained by the highly localized state of bound excitons that are trapped by surface impurities on TMD. Our finding can break ground on a novel stage of TMD investigation that deals with atomic scale impurity physics

* Address correspondence to kato12@ecei.tohoku.ac.jp.

Received for review October 20, 2014 and accepted December 3, 2014.

Published online December 03, 2014
10.1021/nn5059858

© 2014 American Chemical Society

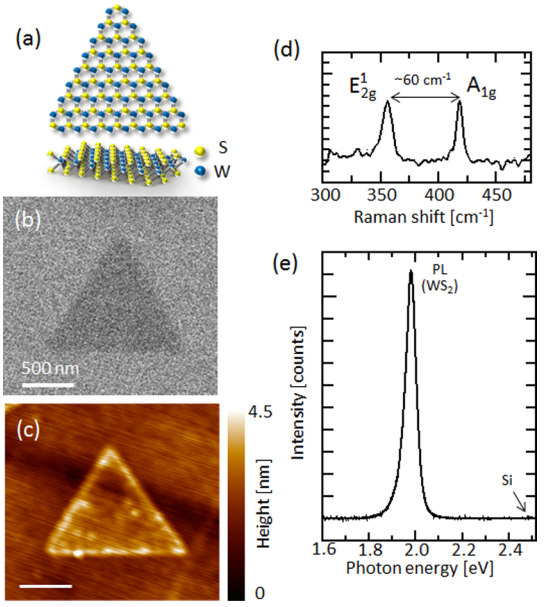

Figure 1. (a) Schematic illustration of monolayer and single crystal WS_2 structure; typical (b) SEM and (c) AFM images of WS_2 triangle crystals grown by CVD; (d) Raman scattering spectrum; and (e) PL spectrum of WS_2.

and engineering, which is expected to contribute to the future development of TMD-based quantum optical science and its applications.

RESULTS AND DISCUSSION

The WS_2 sample was grown by a conventional chemical vapor deposition (CVD) method (see the Methods section).[16] Figure 1 shows the structural model (Figure 1a), a typical SEM image (Figure 1b), and AFM image (Figure 1c) of a single crystal monolayer WS_2 sample. The crystals were observed to have a triangular shape with ~1 nm thickness. The E^1_{2g} and A_{1g} Raman modes were obtained with ~60 cm^{-1} peak difference (Figure 1d). Bright PL spectra were obtained from the triangularly shaped WS_2 sample. The PL intensity was over 100 times brighter than that of the Raman scattering spectrum from a silicon substrate (Figure 1e). These data are consistent with the features of monolayer and single crystal WS_2.[16,17]

Detailed PL measurements were then carried out on the CVD grown single crystal WS_2. All of the PL spectra were measured under low temperature (83 K) and vacuum (<0.2 Pa) conditions, unless otherwise noted. In most cases, the PL spectrum of the WS_2 sample can be decomposed into neutral excitons (A) (~2.05 eV) and trions (A^-) (~1.98 eV) by careful fitting with the Gauss–Lorentzian function (Figure 2a). Occasionally, however, another sharp peak (denoted by an "X" in Figure 2b) was observed between 1.8 and 2 eV (Figure 2b). To identify the origin of this peak, PL intensity mapping was carried out *via* confocal microscopy. Careful comparison of PL intensity mapping and AFM images showed that peak X can be observed only from the specific area shown in Figure 2 panels c, d, and e (area P2). To reveal the fine structure in this region, further detailed AFM measurements were carried out for the area (P2), showing that it consists of six triangles of WS_2 (Figure 2f). Phase image (Figure 2g), height image (Figure 2h), and line profile (Figure 2i) of the AFM show that the triangles of WS_2 are connected to each other without layer-by-layer stacking. This indicates that grain boundaries should be formed between each crystal. Since the area (P2) where peak X was observed is well matched with the position of the grain boundary, it can be concluded that peak X corresponds to the grain boundary in WS_2. Similar peaks can be observed in other samples (see Supporting Information). It should be noted that not all positions, but only a specific position in the grain boundaries, can give rise to the characteristic peak X. Peak X sometimes suddenly disappeared during the measurement process. This indicates that the origin of peak X may be associated with a renormalized band state formed by physisorbed surface impurities such as N_2 and O_2 at the grain boundary (discussed later).[15]

Through the systematic measurements conducted, it was found that there is a sample-to-sample variation for the energy of peak X, ranging from 1.8 to 2 eV (Figure 3a). The full width at half-maximum (fwhm) of peak X (Γ_{PLX}) was plotted as a function of peak energy shift from neutral excitons (ΔE_{PL}), as shown in Figure 3 panels b and c. The Γ_{PLX} and ΔE_{PL} are distributed in a much lower energy range than that of the data shown in ref 15 (Figure 3b), which indicates that the origin of peak X should be different from the previously reported one.[15] Figure 3c illustrates the enlarged plot of Figure 3b around the peak X region. The Γ_{PLX}–ΔE_{PL} plot suggests categorizing peak X into two types: type 1, which appears at small ΔE_{PL} (<0.12 eV) with narrow Γ_{PLX} (10–40 meV), and type 2, which appears at large ΔE_{PL} (>0.12 eV) with broad Γ_{PLX} (>50 meV). The origin of the peak X for type 1 and type 2 are subsequently investigated.

According to previous studies on multiple semiconductor materials, there are many kinds of peaks around the lower energy side of neutral free excitons.[18–20] The main features of these peaks are as follows: (1) Bound excitons trapped by a shallow potential. These are associated with a sharp peak width, which is not broadened by an increase in temperature, and a relatively small energy shift from the neutral excitons.[18,19] (2) Bound excitons trapped by a deep potential. These are associated with a broad peak width and a relatively large peak energy shift from neutral excitons.[18,19] (3) Phonon sideband. This is associated with a broad peak width, which is broadened by an increase in temperature, and a peak energy shift from neutral excitons that decreases with an increase in temperature.[20]

In an effort to identify the origin of peak X, we measured the temperature dependence of PL width

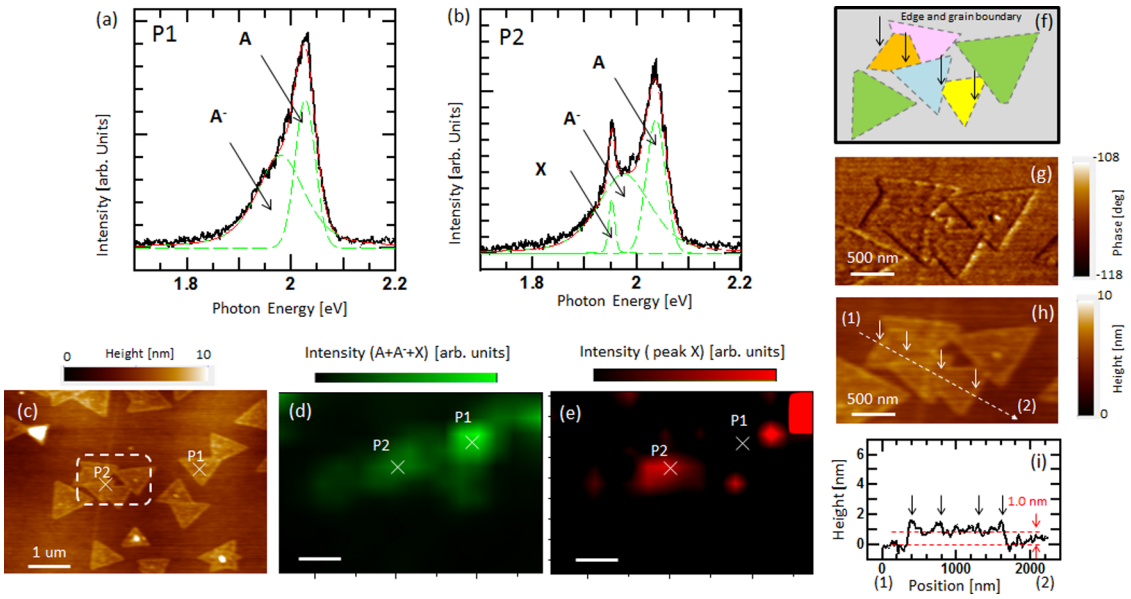

Figure 2. (a,b) The PL spectra of WS_2 taken at (a) P1 and (b) P2 shown in panels c to e. (c) AFM image, PL intensity mapping image of (d) all peaks (A, A^-, X), and (e) peak X of WS_2. (f) Schematic illustration, (g) phase, and (h) height AFM images of WS_2 triangle structure in the P2 region. (i) Line profile of AFM from points 1 to 2 in panel h. Arrows in panels h, f, and I show the position of the grain boundary.

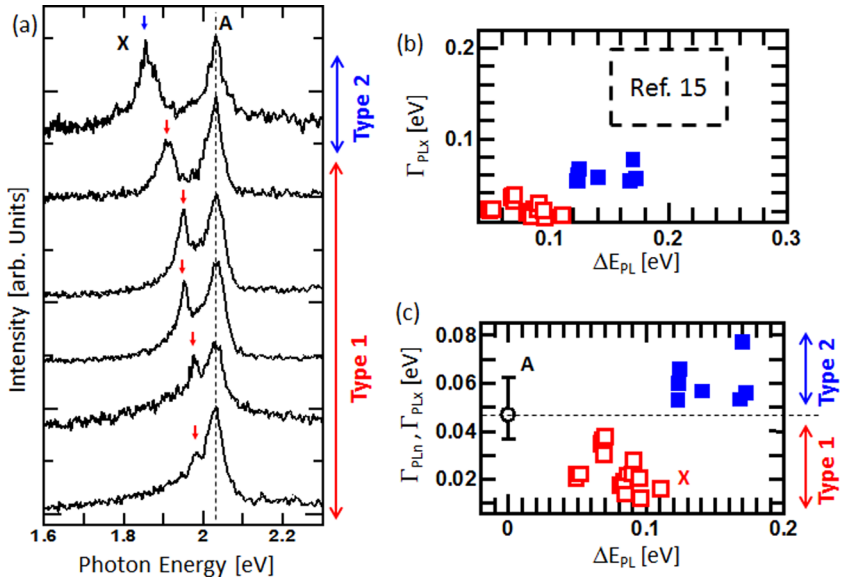

Figure 3. (a) Typical PL spectra of WS_2 taken at the different sample positions. Arrows show the new peak position. (b) Γ_{PLX} (□, type 1; ■, type 2) as a function of ΔE_{PL} with the comparison of data from ref 15 (dashed square region). (c) Enlarged plots of Γ_{PLX} (□, type 1; ■, type 2)−ΔE_{PL}, where the mark ○ denotes the fwhm of neutral excitons (Γ_{PLn}).

and ΔE_{PL}. In the case of type 1, Γ_{PLX} decreases with an increase in temperature (Figure 4a) (discussed later). In contrast, Γ_{PLX} increases with temperature for type 2 (Figure 4b). The increasing of Γ_{PL} with temperature is a well-known phenomenon and can be explained as the result of phonons scattering.[21]

The temperature dependence of ΔE_{PL} was also investigated. For type 2, ΔE_{PL} is not influenced by temperature and decreases monotonically with an increase in temperature by following the conventional Varshni eq (Figure 4d, e).[22] Interestingly, for type 1, the ΔE_{PL} increases with temperature, indicating enhanced localization by temperature increase (discussed as follows) (Figure 4c,e).

These results indicate that peak X cannot be explained by the phonon sideband because ΔE_{PL} was either constant or increased with temperature. Since the peak is sharp with small ΔE_{PL} and broad with large ΔE_{PL}, type 1 and type 2 can be expected to originate from the bound excitons trapped by shallow and deep potentials, respectively.

The best possible explanation of type 1 and type 2 peaks can be summarized by the following model, illustrated in Figure 5. As shown in Figure 2, peak

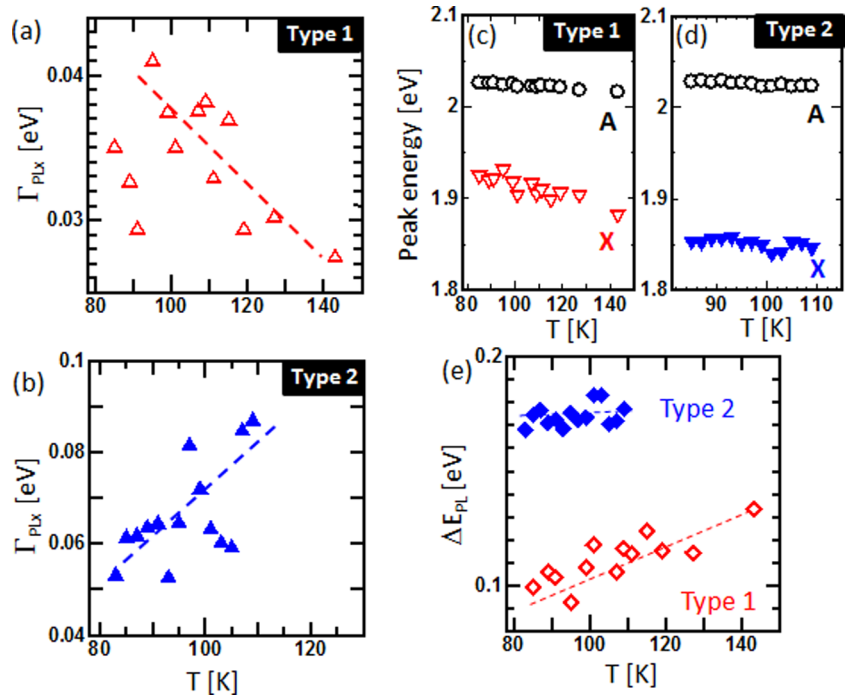

Figure 4. Temperature dependence of (a,b) Γ_{PLX}, (c,d) peak energy, and (e) Δ_{EPL} for (a,c) type 1, (b,d) type 2.

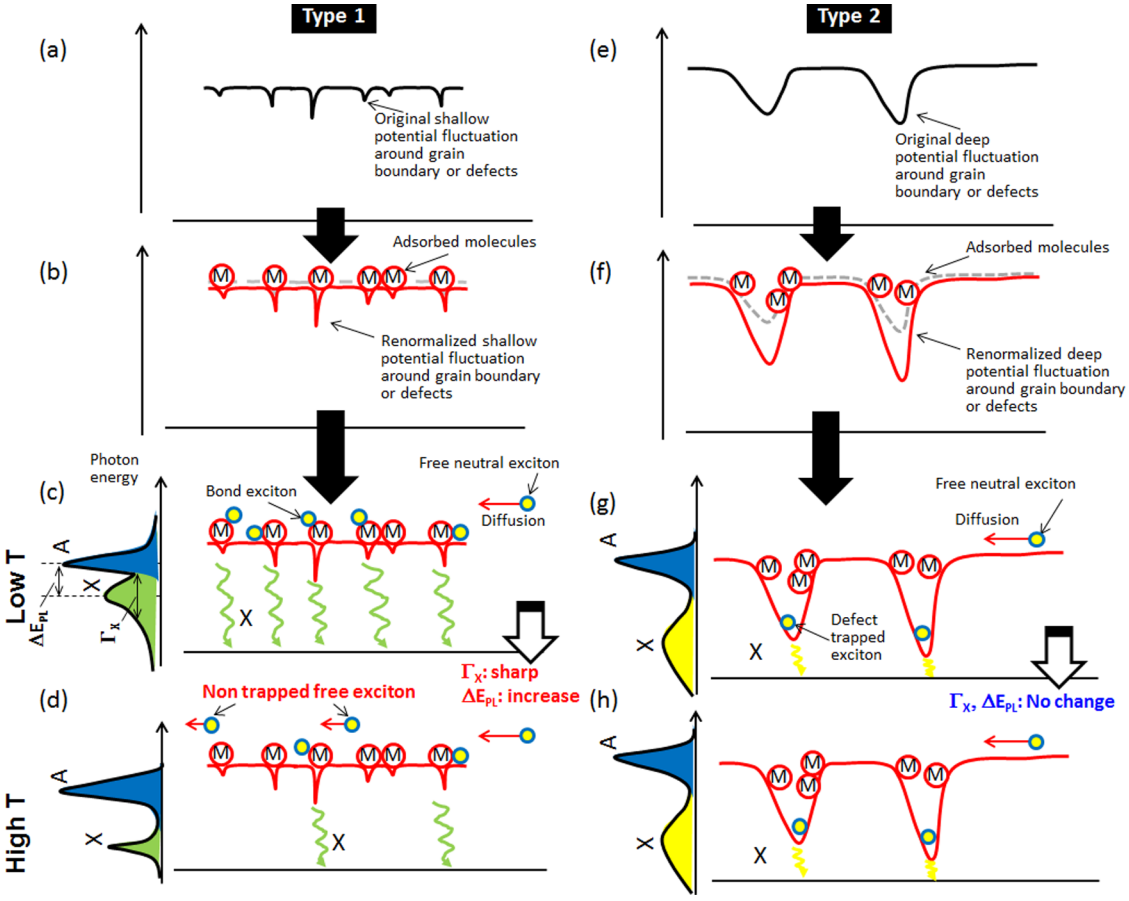

Figure 5. Schematic model for peak X for (a–d) type 1 and (e–h) type 2. Band structure of WS_2 before laser excitation for exciton generation (a,e) without and (b,f) with molecule adsorption. Exciton diffusion kinetics for (c,g) low and (d,h) high temperature after exciton generation for (c,d) type 1 and (g,h) type 2.

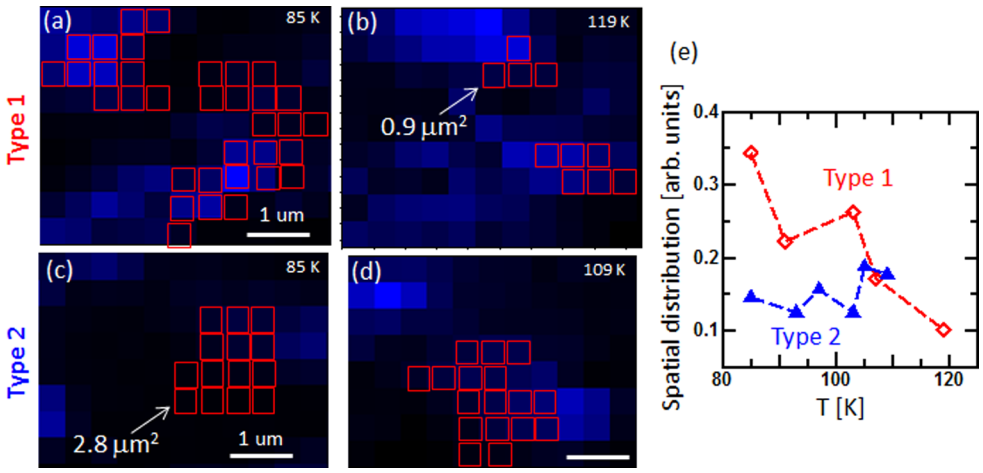

Figure 6. (a–d) I_{PL} mapping at low and high temperature for type 1 and type 2. A red square denotes the spots where peak X was observed. (e) Concentration of peak X spots in measured area as a function of temperature.

X can be observed only from the grain boundary region where certain amounts of potential fluctuations should exist. Once the potential fluctuation is formed (Figure 5a), some impurities (atoms or molecules) can be stabilized by physisorption at the fluctuated potential, and the original band structures of TMD can be renormalized (Figure 5b).[15] For type 1, the shallow potential fluctuations are localized, and therefore generated excitons can be trapped by the surface impurities (not by shallow potential itself) adsorbed at the localized potential. In this case, the trapping efficiency of free excitons by surface impurities should depend on temperature. At low temperature, the free excitons can be efficiently trapped by surface impurities due to the relatively low kinetic energy of free excitons (Figure 5c), whereas the trapping efficiency decreases with an increase in temperature because of the thermal activation of free excitons (Figure 5d). The PL emissions can be explained through the recombination of excitons trapped by the surface impurities. Since such excitons can be formed only at the spots where the binding energy between the surface impurity and free excitons is higher than the kinetic energy of free excitons, the number of trapping sites should decrease with an increase in temperature, and furthermore the localization should be enhanced, resulting in the narrowing of Γ_{PLX} (consistent with Figure 4a). In general, the binding energy of neutral exciton itself (electron–hole binding energy) is known to be estimated from the energy shift between band gap (estimated from optical absorption spectra) and PL peak. Thus, the PL peak of neutral excitons with strong binding energy appears with the large red shift from the band gap energy. A similar tendency can appear for the bound excitons. The PL energy shift for bound excitons (neutral excitons trapped by the impurities) from that of neutral exciton can be directly influenced by the binding energy between impurities and neutral excitons. Thus, ΔE_{PL} here includes the important information for the binding energy between impurity and neutral exciton, that is, the binding energy of bound excitons. A higher binding energy is required to form surface-impurity-trapped bound excitons at high temperature, resulting in the increase of ΔE_{PL} with temperature (consistent with Figure 4c,d).

For the case of type 2, deep potential fluctuations should exist in relatively large surface regions (Figure 5e) where physisorbed impurities can renormalize the band structures (Figure 5f), just as in the case of type 1.[15] At this point, free excitons can be trapped in the deep potential around the defect where it is more energetically stable than forming bound excitons with the surface impurities (Figure 5g). The excitons trapped by the deep potentials are stable and show a weak temperature dependence of Γ_{PLX} and ΔE_{PL} (Figure 5h), which is consistent with Figure 4 panels d and e.

To confirm the accuracy of the explanation given above and depicted in Figure 5, the spatial distributions of peak X were measured at various temperatures by confocal PL mapping (all mapping data are shown in the Supporting Information). Each measurement was carried out with 400 nm step mapping at the same region in the same sample. The red squares in the integrated PL intensity map indicate the spots where peak X can be observed (Figure 6 panels a–d). For type 1 (Figure 6a,b,e), spatial distribution gradually decreased with an increase in temperature. Moreover, only several spots can clearly show peak X at a relatively high temperature condition (119 K) (Figure 6b). By way of contrast, the distribution for type 2 varied little with an increase in temperature (Figure 6c–e). Since the trapping rate of free excitons captured by the adsorbed impurities can decrease with thermal activation, the number of peak X spots should decrease with a temperature increase for type 1, whereas the trapping rate of free excitons by the deep potential around defects does not change with temperature. This results

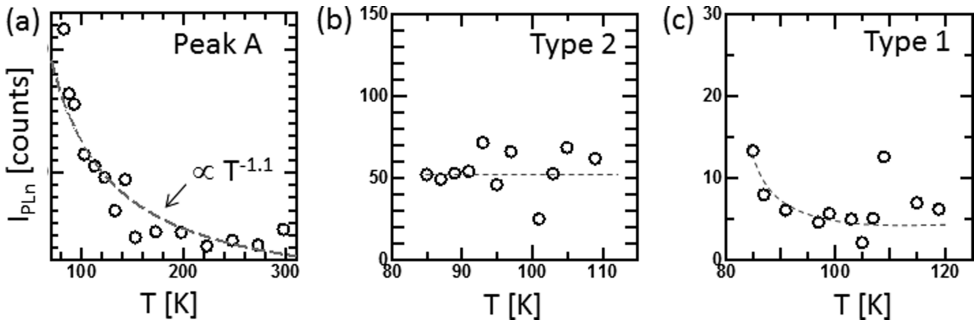

Figure 7. Temperature dependence of I_{PL} for (a) peak A measured at in-plane area, (b) type 2, and (c) type 1.

in an almost constant spatial distribution of peak X with temperature increase for type 2. These data are consistent with the temperature dependence of Γ_{PL} (Figure 4a,b), ΔE_{PL} (Figures 4c,e), and the model shown in Figure 5. It should be also mentioned that the size of the emission site is different for type 1 and type 2. When we estimate the minimum scale of emission spot from the PL mapping results, it is about 0.9 μm^2 and 2.8 μm^2 for type 1 and type 2, respectively. Although the spatial resolution of PL mapping is not enough to discuss the atomic scale structures, it can be conjectured that the defect for type 1 can include relatively smaller scale structures than that of type 2.

Further important information relating to the dimension of excitons for type 1 and type 2 can be obtained from the temperature dependence of integrated PL intensity (I_{PL}). The I_{PL} of excitons in the N-(0-, 1-, 2-) dimension is proportional to their N-dimension radiative decay rate k_{ND} and the population of excitons n_{ex} as $I_{PL} \propto k_{ND} n_{ex}$.[23] Note that k_{ND} depends on T^0 (constant), $T^{-1/2}$, and T^{-1} for 0, 1, and 2 dimensions, respectively, which arises from the N-dimension density of states (DOS) and their thermalization within the exciton band.[23,24]

The T-dependence of I_{PL} was measured at the in-plane region of the sample, where peak X cannot be observed. In this case, the I_{PL} tends to follow the $T^{-\gamma}$ curve with $\gamma \approx 1.1$. Because the density of neutral excitons (n_{exn}) should be proportional to the laser excitation power, and should be independent of T, the radiative decay rate of neutral excitons (k_{NDn}) can be proportional to $T^{-1.1}$ (Figure 7a). This suggests that the motion of neutral excitons in the WS_2 sample can be well described as free excitons in 2D structures. The I_{PL} of type 1 and type 2 were then investigated as a function of temperature. Interestingly, type 2 does not show clear temperature dependence, that is, $\propto T^0$ (Figure 7b). This indicates that the excitons for type 2 have 0D motion,[23] providing further evidence that type 2 originates from the localized bound excitons. The PL intensity of type 1 noticeably decreased with the temperature increase (Figure 7c). This can be explained by the temperature dependence of densities of bound excitons. As explained in Figure 5 and Figure 6, the trapping rate of free excitons with the surface impurities decreases with an increase in temperature. This indicates that the generation rate of bound excitons decreased with temperature, resulting in the depletion of I_{PL} with temperature increase. This is consistent with the previous report for bound excitons trapped by the shallow potential in other semiconductor materials.[25,26] Since ΔE_{PL}, a sign of the binding energy between impurities and excitons, is high (Figure 3c), type 2 bound excitons are more stable than type 1 excitons. Therefore, detrapping of neutral excitons by thermal activation with temperature increase can be negligible for type 2 excitons at least in this temperature range (83−300 K) (Figure 5).

On the basis of these results relating to the temperature dependence of Γ_{PL} (Figure 4a,b), ΔE_{PL} (Figure 4c−4e), spatial distribution (Figure 6), and I_{PL} (Figure 7), we can conclude that the origin of type 1 and type 2 peaks concerns bound excitons trapped by the shallow and deep potential fluctuations, respectively. Since the peak width of type 1 is very narrow (10−40 meV) at low temperature (83 K), the state of type 1 excitons should be highly localized, possibly at the scale of single or several molecules. This is the first report optically revealing the existence of the impurity state with strong localizations in TMD.

As we have demonstrated above, type 1 can be identified as bound excitons trapped by surface impurities with strong localization. We now attempt to discuss possible candidates for the kind of impurities responsible for trapping the excitons. As Tongay *et al.* reported, physisorbtion of molecules such as nitrogen and oxygen strongly affects the band state of TMD.[15] In response to this report, systematic investigations were carried out to study the effects of physisorbed molecules. At first, as-grown WS_2 with relatively high crystallinity was used. The PL intensity was measured under vacuum conditions, as well as in the presence of N_2 (2000 Pa), and O_2 (2000 Pa), at a low temperature (83 K). Compared with the case of the vacuum, certain values of increase can be observed in I_{PL} under the presence N_2 and O_2. However, the peak X cannot be observed in any spots (see Supporting Information). We then used a WS_2 sample including a certain

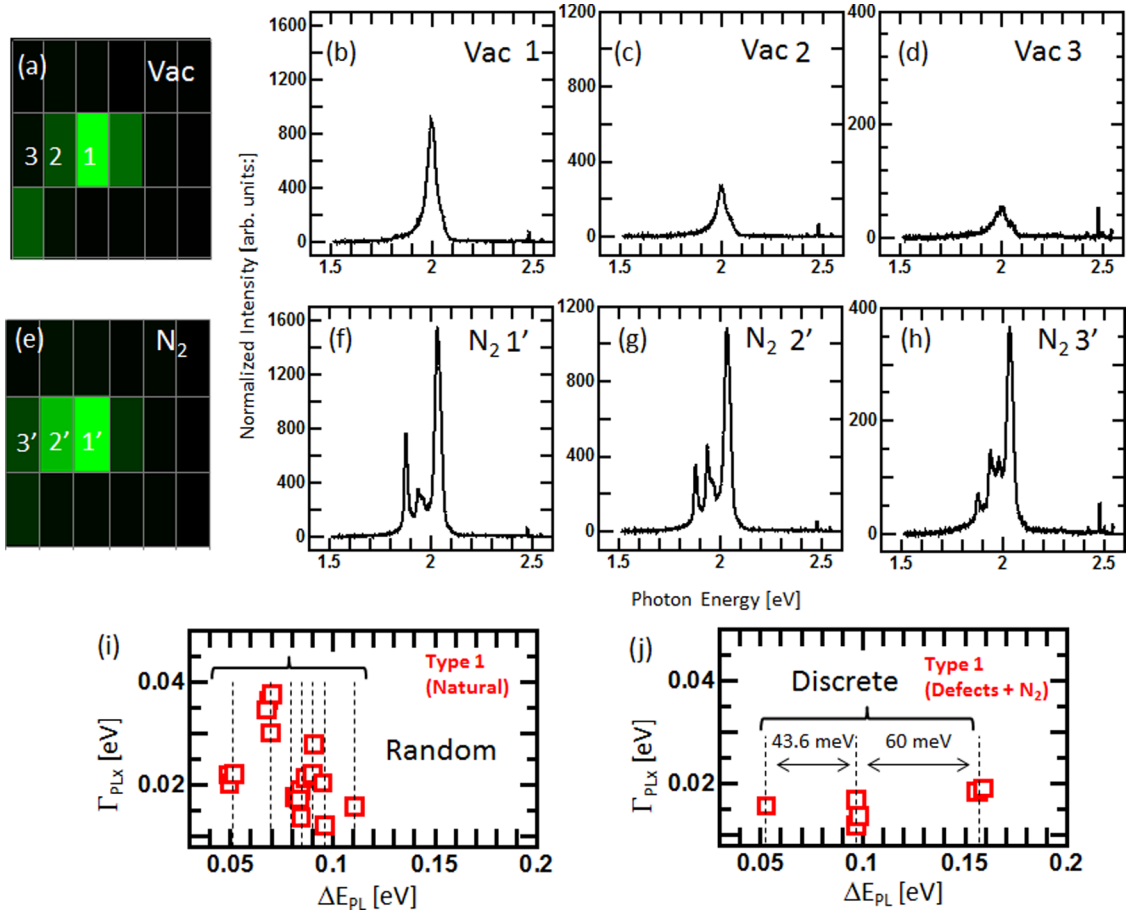

Figure 8. (a,e) I_{PL} mapping image and (b−d, f−h) raw PL spectra of defect-induced WS_2 taken under the (a−d) vacuum and (e−h) N_2 conditions at 83 K. (i, j) Enlarged plot of type 1 Γ_{PLX} as a function of ΔE_{PL} measured (i) under the vacuum with as-grown WS_2 (natural grain boundary defect) and (j) under the N_2 atmosphere (2000 Pa) with defect-induced WS_2. Dashed lines denote the distribution of ΔE_{PL}.

amount of defects. The defects were created by exposing the sample to vapor from boiled water. In this case, the I_{PL} drastically increased with an increase in the N_2 pressure. At suitable conditions, the I_{PL} increased by a factor of almost 10, compared to its value before the N_2 exposure. With an increase in the N_2 pressure, the integrated intensity ratio of neutral excitons to trions (I_A/I_A^-) gradually increased, and the peak position of neutral excitons increased (see Supporting Information). These features show that the adsorption of N_2 molecules on the surface of the WS_2 sample caused the neutralization of trions, resulting in the drastic increase of I_A.[15] Furthermore, peak X can often be clearly observed for the defect-induced sample under the presence of N_2 (Figure 8). On the basis of the plot of peak width vs energy shift from the neutral exciton peak, all of the peak X in Figure 8 are distributed in the very narrow peak width region (0.01−0.02 eV), which is similar to that of type 1 (0.01−0.04 eV) shown in Figure 2. Although several peaks show slightly larger energy shifts (0.15 eV) than that of type 1 in Figure 2 (~0.12 eV), it can be explained by the difference of exciton binding states within the localized states. This indicates that the localized excitons formed at naturally formed grain boundary defects (Figures 2 and 3) and externally introduced defects by water vapor exposure with N_2 adsorption (Figures 8, S4) should have almost the same optical state even though the measurement condition was not exactly the same.

As we show in Figure 2, the peak energy was slightly varied even in the type 1 peaks. This can be caused by the deviation of impurity species. Interestingly, when we introduced the N_2 under the vacuum condition, the deviation of peak energy drastically decreased, and ΔE_{PL} degenerated into three energy states as shown in Figure 8(i, j). The explanation for this is that the deviation of peak energy for type 1 can be suppressed by decreasing the kinds of adsorbed species. Although the reason for the multipeaks in Figure 8 is not clear, it can be supposed that the band structures of the defect with a large amount of N_2 adsorption may be degenerated into several different states with about several tens of meV energy separations, which may appear as different trapping states for type 1 excitons. This implies that the fine band structures at the defects may be investigated from the multiple type 1 peaks, which is the next topic of this study.

Similar effects can be also observed under the presence of O_2. This indicates that the defective site is necessary to stabilize the physisorbtion of molecules such as N_2 and O_2, and that these molecules play an essential role as the trapping center of free excitons, which gives rise to impurity-trapped bound excitons. Note that the type 1 peak can be often observed around the grain boundary region rather than the defective area at the in-plane region. This may indicate that the shallow potential fluctuation can be dominantly formed around the grain boundary region. The defects at the in-plane region may easily cause the deep potential fluctuation resulting in the formation of type 2 bound excitons.

Finally, we discuss the state of the surface impurities on the WS_2 sample by considering the effective mass model. It is known that there are requisite conditions to trap the free excitons by the ionized impurities. For the ionized donors, the effective mass ratio of electron (m_e^*) to hole (m_h^*) (m_e^*/m_h^*) should be <0.43, whereas a m_e^*/m_h^* ratio greater than 2.33 is required to trap the free excitons by the ionized acceptors.[27] Since the m_e^*/m_h^* ratio of WS_2 is 0.75,[28] both conditions of ionized donors and acceptors cannot be satisfied, indicating that the surface impurities exist with the neutral state. Furthermore, as discussed above, the N_2 and O_2 adsorptions enhance the formation of bound excitons, and such molecules play a role as electron acceptors for WS_2. Thus, it can be conjectured that the surface impurities forming the bound excitons with strong localization should exist with the neutral acceptor state on the surface of WS_2.

CONCLUSION

A novel PL peak has been observed in WS_2. Detailed temperature dependence measurements of PL width, peak energy, spatial distributions, and integrated intensities have been reported. On the basis of these measurements, we conclude that the peak is the result of bound excitons trapped by the surface impurities, which is completely different from the feature of previously reported bound excitons trapped by the defects. The bound excitons trapped by the surface impurities exhibit very narrow (~10 meV) PL spectra width at low temperature (83 K), showing the trapping state to be highly localized. This finding of the optically detectable localized impurity state in TMD exhibits the promising potential to expand the study of TMD for atomic impurity physics and engineering, with applications ultimately residing in the realm of quantum optics.

METHODS

Material Synthesis. The WS_2 was grown by a conventional chemical vapor deposition (CVD) method.[16] Thin WO_3 film was first deposited on a SiO_2 substrate *via* vacuum evaporation. The substrate was then heated up to the desired temperature (700−900 °C) and sulfur vapor introduced to cause chemical reaction of $2WO_3 + 7S = 2WS_2 + 3SO_2$, resulting in the formation of monolayer and single crystal WS_2.

Characterizations. The structure of the WS_2 sample was characterized by atomic force microscopy (AFM; JEOL, JSPM-5400, Japan), scanning electron microscopy (SEM; Hitachi, SU1510, Japan), Raman scattering spectroscopy, and PL spectroscopy. PL measurements were carried out by confocal Raman/PL microscopy (Horiba, HR 800, Japan) with 488 nm laser excitation. The temperature of the sample was controlled by low-temperature stage units (Japan High Tech, 10086L, Japan).

Conflict of Interest: The authors declare no competing financial interest.

Supporting Information Available: Novel peak for other samples; more data for spatial distribution of peak X; effects of gas adsorption on PL spectra for as-grown and defect-induced WS_2. This material is available free of charge *via* the Internet at http://pubs.acs.org.

Acknowledgment. This work was supported in part by Grant-in-Aid for Young Scientists A (Grant No. 25706028), Grant-in-Aid for Scientific Research on Innovative Areas (Grant No. 26107502) from JSPS KAKENHI, the Murata Science Foundation, and the Cooperative Research Project Program of the Research Institute of Electrical Communication, Tohoku University.

REFERENCES AND NOTES

1. Kane, B. E. A Silicon-Based Nuclear Spin Quantum Computer. *Nature* **1998**, *393*, 133–137.
2. Vrijen, R.; Yablonovitch, E.; Wang, K.; Jiang, H. W.; Balandin, A.; Roychowdhury, V.; Mor, T.; Divincenzo, D. Electron-Spin-Resonance Transistors for Quantum Computing in Silicon−Germanium Heterostructures. *Phys. Rev. A* **2000**, *62*, 012306-1–10.
3. Hollenberg, L. C.; Dzurak, A. S.; Wellard, C.; Hamilton, A. R.; Reilly, D. J.; Milburn, G. J.; Clark, R. G. Charge-Based Quantum Computing Using Single Donors in Semiconductors. *Phys. Rev. B* **2004**, *69*, 113301-1–4.
4. Kurtsiefer, C.; Mayer, S.; Zarda, P.; Weinfurter, H. Stable Solid-State Source of Single Photons. *Phys. Rev. Lett.* **2000**, *85*, 290–293.
5. Muller, A.; Bianucci, P.; Piermarocchi, C.; Fornari, M.; Robin, I. C.; André, R.; Shih, C. K. Time-Resolved Photoluminescence Spectroscopy of Individual Te Impurity Centers in ZnSe. *Phys. Rev. B* **2006**, *73*, 081306-1–4.
6. Ikezawa, M.; Sakuma, Y.; Masumoto, Y. Single Photon Emission from Individual Nitrogen Pairs in GaP. *Jpn. J. Appl. Phys.* **2007**, *46*, L871–L873.
7. Strauf, S.; Michler, P.; Klude, M.; Hommel, D.; Bacher, G.; Forchel, A. Quantum Optical Studies on Individual Acceptor Bound Excitons in a Semiconductor. *Phys. Rev. Lett.* **2002**, *89*, 177403-1–4.
8. Beveratos, A.; Kühn, S.; Brouri, R.; Gacoin, T.; Poizat, J.-P.; Grangier, P. Room Temperature Stable Single-Photon Source. *Eur. Phys. J. D* **2002**, *18*, 191–196.
9. Koenraad, P. M.; Flatté, M. E. Single Dopants in Semiconductors. *Nat. Mater.* **2001**, *10*, 91–100.
10. Splendiani, A.; Sun, L.; Zhang, Y.; Li, T.; Kim, J.; Chim, C.-Y.; Galli, G.; Wang, F. Emerging Photoluminescence in Monolayer MoS_2. *Nano Lett.* **2012**, *10*, 1271–1275.
11. Radisavljevic, B.; Radenovic, A.; Brivio, J.; Giacometti, V.; Kis, A. Single-Layer MoS_2 Transistors. *Nat. Nanotechnol.* **2011**, *6*, 147–150.
12. Mak, K. F.; He, K.; Shan, J.; Heinz, T. F. Control of Valley Polarization in Monolayer MoS_2 by Optical Helicity. *Nat. Nanotechnol.* **2012**, *7*, 494–498.

13. Cao, T.; Wang, G.; Han, W.; Ye, H.; Zhu, C.; Shi, J.; Niu, Q.; Tan, P.; Wang, E.; Liu, B.; Feng, J. Valley-Selective Circular Dichroism of Monolayer Molybdenum Disulphide. *Nat. Commun.* **2012**, *3*, 887-1–5.
14. Xiao, D.; Liu, G.-B.; Feng, W.; Xu, X.; Yao, W. Coupled Spin and Valley Physics in Monolayers of MoS_2 and Other Group-VI Dichalcogenides. *Phys. Rev. Lett.* **2012**, *108*, 196802-1–5.
15. Tongay, S.; Suh, J.; Ataca, C.; Fan, W.; Luce, A.; Kang, J. S.; Liu, J.; Ko, C.; Raghunathanan, R.; Zhou, J.; Ogletree, F.; Li, J.; Grossman, J. C.; Wua, J. Defects Activated Photoluminescence in Two-Dimensional Semiconductors: Interplay between Bound, Charged, and Free Excitons. *Sci. Rep.* **2013**, *3*, 2657-1–5.
16. Gutiérrez, H. R.; Perea-López, N.; Elías, A. L.; Berkdemir, A.; Wang, B.; Lv, R.; López-Urías, F.; Crespi, V. H.; Terrones, H.; Terrones, M. Extraordinary Room-Temperature Photoluminescence in Triangular WS_2 Monolayers. *Nano Lett.* **2012**, *13*, 3447–3454.
17. Zhao, W.; Ghorannevis, Z.; Chu, L.; Toh, M.; Kloc, C.; Tan, P.-H.; Eda, G. Evolution of Electronic Structure in Atomically Thin Sheets of WS_2 and WSe_2. *ACS Nano* **2013**, *7*, 791–797.
18. Haynes, J. R. Experimental Proof of the Existence of a New Electronic Complex in Silicon. *Phys. Rev. Lett.* **1960**, *4*, 361–363.
19. Pelant, I.; Valenta, J. *Luminescence Spectroscopy of Semiconductors*; Oxford Univ. Press: Cambridge, UK, 2012; p 181.
20. Xua, S. J.; Li, G. Q.; Xiong, S.-J.; Che, C. M. Temperature Dependence of the LO Phonon Sidebands in Free Exciton Emission of GaN. *J. Appl. Phys.* **2006**, *99*, 073508-1–5.
21. Lee, J.; Koteles, E. S.; Vassell, M. O. Luminescence Linewidths of Excitons in GaAs Quantum Wells below 150 K. *Phys. Rev. B* **1986**, *33*, 5512–5516.
22. Varshni, Y. P. Temperature Dependence of the Energy Gap in Semiconductors. *Physica* **1967**, *34*, 149–154.
23. Mouri, S.; Miyauchi, Y.; Iwamura, M.; Matsuda, K. Temperature Dependence of Photoluminescence Spectra in Hole-Doped Single-Walled Carbon Nanotubes: Implications of Trion Localization. *Phys. Rev. B* **2013**, *87*, 045408-1–4.
24. Akiyama, H.; Koshiba, S.; Someya, T.; Wada, K.; Noge, H.; Nakamura, Y.; Inoshita, T.; Shimizu, A.; Sakaki, H. Thermalization Effect on Radiative Decay of Excitons in Quantum Wires. *Phys. Rev. Lett.* **1994**, *72*, 924–927.
25. Viswanath, A. K.; Lee, J. I.; Yu, S.; Kim, D.; Choi, Y.; Hong, C.-H. Photoluminescence Studies of Excitonic Transitions in GaN Epitaxial Layers. *J. Appl. Phys.* **1998**, *84*, 3848–3859.
26. Teke, A.; Özgür, U.; Dogan, S.; Gu, X.; Morkoç, H.; Nemeth, B.; Nause, J.; Everitt, H. O. Excitonic Fine Structure and Recombination Dynamics in Single-Crystalline ZnO. *Phys. Rev. B* **2004**, *70*, 195207-1–10.
27. Pelant, I.; Valenta, J. *Luminescence Spectroscopy of Semiconductors*; Oxford Univ. Press: Cambridge, UK, 2012; p 183.
28. Liu, L.; Kumar, S. B.; Ouyang, Y.; Guo, J. Performance Limits of Monolayer Transition Metal Dichalcogenide Transistors. *IEEE Trans. Electron Devices* **2011**, *58*, 3042–3047.